Catalytic H_2 Production

International Edition: DOI: 10.1002/anie.201508351
German Edition: DOI: 10.1002/ange.201508351

Development of a Dinitrosyl Iron Complex Molecular Catalyst into a Hydrogen Evolution Cathode

Tzung-Wen Chiou, Tsai-Te Lu,* Ying-Hao Wu, Yi-Ju Yu, Li-Kang Chu, and Wen-Feng Liaw**

Abstract: *Despite extensive efforts, the electrocatalytic reduction of water using homogeneous/heterogeneous Fe, Co, Ni, Cu, W, and Mo complexes remains challenging because of issues involving the development of efficient, recyclable, stable, and aqueous-compatible catalysts. In this study, evolution of the de novo designed dinitrosyl iron complex DNIC-PMDTA from a molecular catalyst into a solid-state hydrogen evolution cathode, considering all the parameters to fulfill the electronic and structural requirements of each step of the catalytic cycle, is demonstrated. DNIC-PMDTA reveals electrocatalytic reduction of water at neutral and basic media, whereas its deposit on electrode preserves exceptional longevity, 139 h. This discovery will initiate a systematic study on the assembly of [Fe(NO)$_2$] motif into current collector for mass production of H_2, whereas the efficiency remains tailored by its molecular precursor [(L)Fe(NO)$_2$].*

Dihydrogen has emerged as a clean, renewable, and sustainable energy to remedy the environmental pollution from CO_2-accumulation and energy shortage in the future.[1] Bacterial hydrogenases are known to harbor diiron catalytic centers, in conjunction with iron-sulfur clusters, for the reduction of water as part of the respiration process.[2] Electrocatalytic H_2-generation from water at pH 7 using precious platinum electrodes can overcome the O_2-intolerance of [Fe-Fe]-hydrogenase, and lower the onset potential, −430 mV, compared to −400 mV (vs. SHE) observed in [Fe-Fe]-hydrogenase.[3,4] Considering the industrial applications, Fe, Co, Ni, Cu, W, and Mo metal compounds were assembled into current collectors to create solid-state hydrogen evolution cathodes in the attempt to replace Pt electrodes.[5–9] However, systematic optimization of the cathode is hampered by the difficulty in identifying and quantifying the active species.

From a molecular approach, comprehensive characterization of a catalyst provides insights into the reaction mechanism and to the design of improved catalysts. On the way to explore a robust, efficient, and economical catalyst for H_2-generation from water as an ultimate goal, complexes $[Fe_2(\mu\text{-}S_2(CH_2)_3(CO)_4(L)_2]$ (L = PMe_3, CN^-) were first reported as a [Fe-Fe]-hydrogenase active-site model featuring electrocatalytic H_2-generation activity in acidic organic solution.[10–12] Mechanistic study of both [Fe-Fe]-hydrogenase and biomimetic models, with a parallel progress in sophisticated ligand design and synthesis, lead to the development of bioinspired Co, Ni, and Mo complexes for electrocatalytic and photocatalytic H_2-generation in aqueous solution.[3,13–19] Development of these biomimetic and bioinspired catalysts discloses the requirements of a reversible two-electron redox process, a low-valence metal center, aqueous compatibility, and the capability of providing exchangeable coordination sites to accommodate water, hydride, and dihydrogen for efficient catalysts of electrocatalytic H_2-generation from water. Incorporation of an appropriate proton-transfer pathway further enhanced the catalytic efficiency.[13] However, a recyclable molecular catalyst featuring long-term stability, wide working pH-range, and compatibility with diverse water source (seawater in particular), suitable for practical application in H_2-generation has not yet been reported (Supporting Information, Table S1).

Dinitrosyl iron complexes (DNICs), identified as a degradation product of nitrosylating [Fe-S] proteins, exhibit reversible redox interconversion between $\{Fe(NO)_2\}^9$ and $\{Fe(NO)_2\}^{10}$ DNICs.[20,21] The superscript represents the summation of electrons in Fe 3d orbitals and NO π* orbitals according to the Enemark–Feltham notation.[22] Development of a variety of DNICs through facile synthetic procedures and extensive spectroscopic study unveiled regulation of the redox potential and intrinsic electron transfer between Fe and NO within DNICs by its nuclearity, geometric structure, and supporting ligands.[20,23–26]

With regard to the inspirational study of bioinspired catalysts, we adopted DNIC as an innovative complex for H_2-generation, relying on its $\{Fe(NO)_2\}^9/\{Fe(NO)_2\}^{10}$ redox couple and transient reduction of $\{Fe(NO)_2\}^{10}$ only achieved in aqueous solution. Herein, structural and spectroscopic characterization reveals how pentamethyldiethylenetriamine (PMDTA), in comparison with tetramethylethylenediamine (TMEDA) and diethylenetriamine (DTA), optimizes the electronic and geometric structure of a [Fe(NO)$_2$] core-containing complex (DNIC-PMDTA) to initiate electrocatalytic H_2 generation in neutral 1.0 M KCl solution. In particular, DNIC-PMDTA deposited on an electrode through extended electrolysis features a low onset potential of −717 mV, a Tafel slope of 202 mV dec^{-1}, and remarkable longevity with an average current density of 246 mA cm^{-2} for 139 h in neutral 1.0 M KCl solution. From a molecular catalyst to a solid-state hydrogen evolution cathode, the [Fe(NO)$_2$] motif represents

[*] Dr. T.-W. Chiou, Y.-H. Wu, Y.-J. Yu, Prof. L.-K. Chu, Prof. W.-F. Liaw
Department of Chemistry, National Tsing Hua University
No. 101, Section 2, Guangfu Rd., Hsinchu, 30013 (Taiwan)
E-mail: d9623817@oz.nthu.edu.tw
wfliaw@mx.nthu.edu.tw
Prof. T.-T. Lu
Department of Chemistry, Chung Yuan Christian University
No. 200, Chung Pei Rd. Taoyuan, 32023 (Taiwan)
E-mail: TTLu@cycu.edu.tw

Supporting information for this article is available on the WWW under http://dx.doi.org/10.1002/anie.201508351.

a translational molecular platform for efficient and long-term generation of H_2 under alternative conditions, whereas the supporting ligands preserve the possibility for the systematic design and improvement of the catalytic efficiency.

$[(NO)_2Fe(TMEDA)]$ (1-TMEDA) was selected as a lead compound to test the electrochemical reactivity of DNICs toward water. 1-PMDTA was synthesized through the reaction of $Fe(CO)_2(NO)_2$ with PMDTA to explore the kinetic role of pendant amines (Scheme 1). 1-DTA, a non-methyl

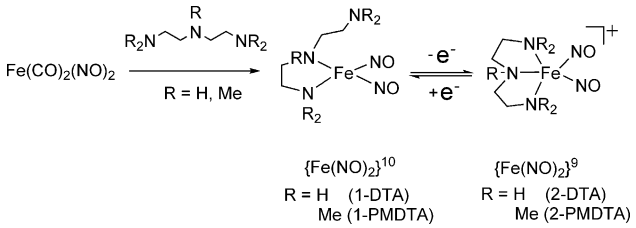

Scheme 1. Synthesis of $\{Fe(NO)_2\}^{10}$ DNICs 1-DTA/1-PMDTA and $\{Fe(NO)_2\}^9$ DNICs 2-DTA/2-PMDTA.

version of 1-PMDTA, was synthesized in a similar manner to contrast the electronic optimization of the redox reactivity of DNICs toward water reduction. Cyclic voltammograms of 2 mM solution of $[(NO)_2Fe(PMDTA)]^+$ (2-PMDTA), $[(NO)_2Fe(DTA)]^+$ (2-DTA), and 1-TMEDA in CH_3CN with 0.1M of $[nBu_4N][PF_6]$ electrolyte, indicate the electrochemical conversion of $\{Fe(NO)_2\}^9$ DNICs to $\{Fe(NO)_2\}^{10}$ DNICs at $E_{pc} = -1.19$, -0.98, and -0.58 V, respectively, versus Fc/Fc^+ (Figure 1A; Supporting Information, Figure S1, Table S2). No other reductive peak was observed beyond $\{Fe(NO)_2\}^{10}$ DNICs in the accessible electrochemical window of CH_3CN. Since 2-PMDTA is unstable in several buffer solutions, KCl is chosen as an electrolyte for electrochemical study. To our surprise, an aqueous solution of 1 mM 2-PMDTA with 0.1M $KCl_{(aq)}$ exhibits a reduction response as a tail rising up from -0.63 V versus standard hydrogen electrode (SHE), as well as the reduction response at $E_{pc} = -0.47$ V derived from conversion of $\{Fe(NO)_2\}^9$ into $\{Fe(NO)_2\}^{10}$ DNICs (Figure 1B). This onset potential (-0.63 V), higher than the onset potential of -0.5 V for direct reduction of water using Pt as working electrode in 0.1M KCl solution, falls within the normal range of those of the reported homogeneous neutral water-reduction catalysts (overpotential 80–660 mV vs. 130 mV for 2-PMDTA; Supporting Information, Table S1).[3,16–19]

The unprecedented electrocatalytic reactivity of DNICs encouraged us to pursue spectroscopic and crystallographic characterization of DNICs to gain insight into the cooperative effect of NO and supporting ligands on triggering electrocatalytic water reduction. IR ν_{NO} frequencies of 1697 and 1643 cm^{-1} exhibited by 1-PMDTA, compared to 1686 and 1634 cm^{-1} exhibited by 1-DTA, and 1698 and 1644 cm^{-1} exhibited by 1-TMEDA, reveal similar electronic structure of 1-PMDTA and 1-TMEDA as opposed to 1-DTA (Supporting Information, Figure S2).[21] Regarding the similar IR ν_{NO} frequencies exhibited by 1-PMDTA and 1-TMEDA, structural comparison of 1-TMEDA and 1-DTA was achieved to

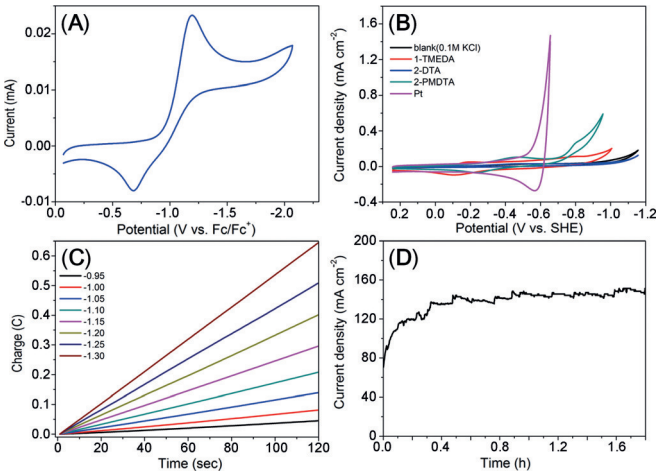

Figure 1. A) Cyclic voltammogram of 2 mM solution of 2-PMDTA in CH_3CN with 0.1 M of $[nBu_4N][PF_6]$ electrolyte. Scan rate: 50 mVs^{-1}. B) Cyclic voltammograms of blank (black), 1 mM aqueous solution of 1-TMEDA (red), 2-DTA (blue), 2-PMDTA (dark green) and Pt (magenta) with 0.1 M of KCl electrolyte. Scan rate: 50 mVs^{-1}. C) Charge consumption by the aqueous solution of 1 mM DNIC 2-PMDTA and 1 M KCl vs. time at different applying potentials (vs. SHE). D) Current density for the electrolysis of 1 mM DNIC 2-PMDTA in 1 M $KCl_{(aq)}$ at an applied potential of -1.2 V (vs SHE).

echo the electronic effect induced by PMDTA ligand, despite the efforts made on crystallographic study of 1-PMDTA. Both $\{Fe(NO)_2\}^{10}$ DNICs with TMEDA and DTA supporting ligands lie in a pseudo-tetrahedral geometry, while a dangling amine group is observed in 1-DTA (Supporting Information, Figure S3). The significantly smaller (O)N–Fe–N(O) bond angle observed in 1-TMEDA provides further insights into the exquisite modulation of the electronic and geometric environment of the $[Fe(NO)_2]$ core to initiate electrocatalytic water reduction. To investigate the kinetic role of the dangling amine group during the catalytic cycle, the redox conversion of DNIC-PMDTA and DNIC-DTA was further explored.

Upon addition of one equiv of $[NO][BF_4]$ to 1-PMDTA, the IR ν_{NO} frequencies shifted from (1697, 1643 cm^{-1}) to (1768, 1683 cm^{-1}), indicating the formation of $\{Fe(NO)_2\}^9$ 2-PMDTA and supported by single-crystal X-ray diffraction (Scheme 1; Supporting Information, Figures S2, S3). Coordination of pendant amine group toward the $\{Fe(NO)_2\}^9$ core in 2-PMDTA by rotation of the C–C bond of ethylene group stabilizes complex 2-PMDTA in a square pyramidal coordination environment with one of the NO ligands occupying the axial position (Supporting Information, Figure S3). Comparable shifts of IR ν_{NO} frequencies, (1686, 1634 cm^{-1}) to (1779, 1702 cm^{-1}), observed in the reaction of $[NO][BF_4]$ and 1-DTA suggest a similar coordination tendency of pendant amine toward the $\{Fe(NO)_2\}^9$ core to afford 2-DTA, with support from single-crystal X-ray diffraction (Supporting Information, Figures S2, S3). Electrochemical, IR, and crystallographic demonstration of $\{Fe(NO)_2\}^9/\{Fe(NO)_2\}^{10}$ DNICs with DTA, PMDTA, and TMEDA ligands discloses that the electronic effect of coordinating ligands initiates the electrocatalytic reactivity of DNIC-PMDTA toward water reduction. Presumably, the dangling amine group serves as a hinge

to shuttle water molecules into the immediate vicinity of $\{Fe(NO)_2\}^{10}$-core, which triggers the transient reduction of $\{Fe(NO)_2\}^{10}$ DNICs to react with water. Subsequently, the pendant amine group is coordinated to the $[Fe(NO)_2]$ core for stabilization of $\{Fe(NO)_2\}^9$ DNICs after evolution of H_2. That is, the chelating PMDTA ligand provides a proton transfer pathway and prevents ligand substitution in the active intermediate state of the electrocatalytic cycle. A thorough spectroscopic study and theoretical calculation for the catalytic mechanism, identification of a Fe-hydride species in particular, is underway.

The catalytic efficacy of 2-PMDTA for H_2-generation was evaluated by controlled potential electrolysis (CPE). Considering the practical applications, CPE experiment was conducted using glassy carbon as the working electrode in the absence of buffer reagents, while 1M KCl was added as electrolyte to minimize internal resistance. Figure 1C shows the charge consumption by 1 mM aqueous solution of 2-PMDTA at different applying potentials. The rate of charge consumption increases with the increasing applying potential. That is, 2.5 mole of H_2 is produced per hour by 1 mole 2-PMDTA using a −1.20 V (vs. SHE) applying potential based on the validated 100% Faradaic efficiency (Supporting Information, Figure S4). To distinguish whether a homogeneous or heterogeneous catalytic process dominates in the catalytic H_2-generation by 2-PMDTA, the dependence of catalytic current on the concentration of 2-PMDTA was measured. The linear relationship between the catalytic current and concentration of 2-PMDTA at potential −1.356 V (vs. SHE; Supporting Information, Figure S5) demonstrates the dominant homogeneous process for the short duration.

Extended electrolysis was further attempted to assess the stability of 2-PMDTA as a practical catalyst for long-term generation of H_2 from water. Regarding the ascending pH value upon reduction of 1M $KCl_{(aq)}$, in which anodic oxidation of Cl^- rather than OH^- and accumulation of OH^- occur, the pH-dependence of catalytic efficacy of 2-PMDTA was evaluated. Despite the decrease of catalytic efficiency with increasing pH, a catalytic current of 1.21 mA at potential −1.356 V (vs. SHE) retained at pH 14, indicating that 2-PMDTA acts as an efficient catalyst for H_2-generation under a wide pH ranges, 7-14 (Supporting Information, Figure S6). We observed that 2-PMDTA is unstable under acidic media. To the best of our knowledge, 2-PMDTA is the first molecular electrocatalyst for hydrogen production effective at pH 14. Figure 1D depicts the current density in the extended electrolysis of 1 mM 2-PMDTA and 1M $KCl_{(aq)}$ at an applying potential −1.2 V (vs. SHE). In particular, current density increases with time from 70 to 140 mA cm^{-2}, and remains steady after 1 h. As a result, a rinse test was pursued to examine the deposit of 2-PMDTA on the electrode surface after this extended electrolysis. DNIC-PMDTA deposited on the electrode after 1 h electrolysis (Supporting Information, Figure S7), in comparison to its precursor DNIC 2-PMDTA, exhibits a lower onset potential and higher catalytic current density for hydrogen-evolution reaction (HER).

Regarding the enhanced HER reactivity featured by the 2-PMDTA-deposited electrode, electrodeposition of DNIC 2-PMDTA on graphite was achieved in a similar fashion for further SEM-EDX, XPS, and solid-state IR characterization. The scanning electron microscopic (SEM) images and pXRD spectra of the fresh graphite electrode and 2-PMDTA-deposited electrode show the coating of amorphous powder on the graphite surface (Figure 2A–C; Supporting Information, Figure S8). No other noble metal elements were observed on the graphite electrode, according to the energy-dispersive X-ray (EDX) spectrum (Figure 2D). Also, SEM-EDX mapping shows that N element (green) is sprinkled over the surface mainly composed of O (red) and Fe (blue) elements (Figure 2E–H). X-ray photoelectron and solid-state IR were adopted to identify the species deposited on the

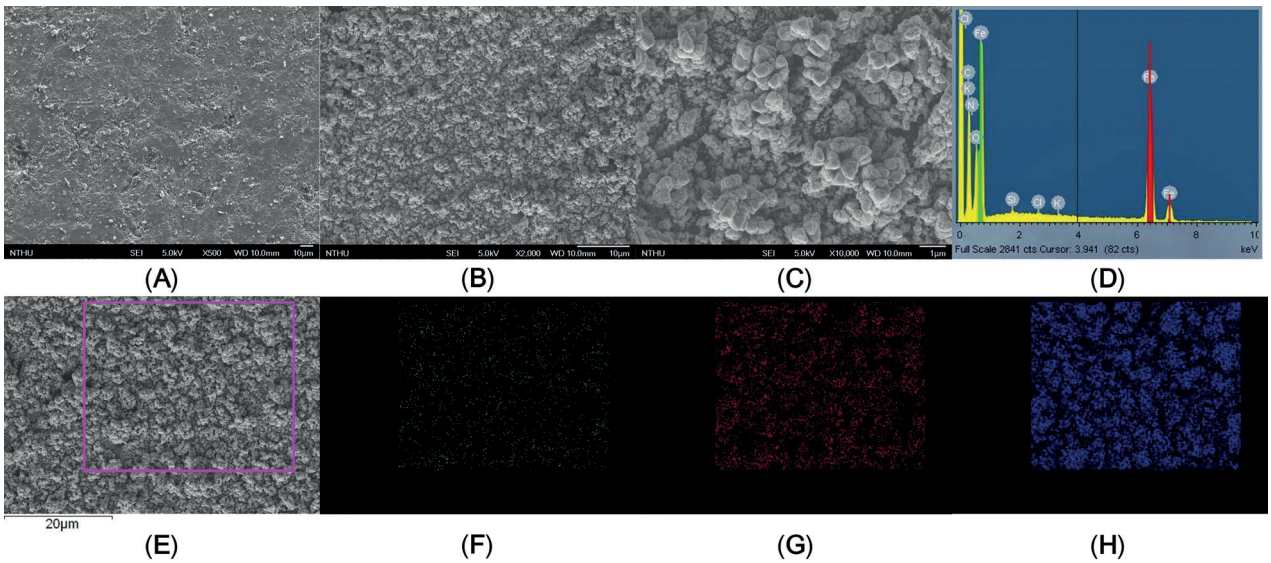

Figure 2. A) SEM image of graphite electrode. B,C) SEM images, D) EDX spectrum and E–H) SEM-EDX elemental maps (N, O, and Fe elements are shown as green, red, and blue, respectively) of 2-PMDTA-deposited electrode.

electrode. A Fe 2p peak at 711.1 eV with a shoulder at 707.4 eV and an O 1 s peak at 530.3 eV with a shoulder at 531.6 eV suggest the deposit of iron metal and iron oxide with surface hydration (Supporting Information, Figure S9). Presumably, an increase in the pH during extended electrolysis (Supporting Information, Figure S10) initiates the degradation of 2-PMDTA under the basic condition and results in the formation of iron oxide deposited on the graphite electrode.[27] The N 1s peak at 400–402 eV resembles the N 1s peak of 2-PMDTA, and indicates the electrodeposition of DNIC-PMDTA onto the electrode surface. On the basis of the quantitative analysis of the XPS, the atomic ratios of N, O, and Fe are 0.98, 33.32, and 10.61, respectively. The IR ν_{NO} stretching frequencies at 1621 and 1721 cm^{-1} observed on the surface of the electrode deviated from the spectrum exhibited by 2-PMDTA in KBr pellet (1641 and 1745 cm^{-1}; Supporting Information, Figure S11), providing further support to the deposit of DNIC-PMDTA on the electrode.[28] Decay of the electrocatalytic reactivity for H_2-generation after the electrode is exposed to air for 24 h indicates that the deposited DNIC-PMDTA dominates the electrocatalytic H_2-generation (Supporting Information, Figure S12). The mechanism and orientation of DNIC-PMDTA deposited on the electrode may perturb its IR ν_{NO} stretching frequencies and requires further investigation.

To unravel the role of the $[Fe(NO)_2]$ motif in the electrodeposition process and how the molecular precursor $[(L)Fe(NO)_2]$ controls the efficiency of the solid-state HER cathode, electrodeposition of 1-TMEDA, 2-DTA, PMDTA, TMEDA, DTA, $FeCl_3$, $FeCl_3$:2PMDTA, $FeCl_3$:2TMEDA, and $FeCl_3$:2DTA, respectively, onto the glassy carbon disk (0.0707 cm^2) was attempted through 1 h electrolysis. Figure S13 A–C (Supporting Information) depict the LSV curves of Pt electrode, Fe electrode, and the modified glassy carbon electrode in 1 M $KCl_{(aq)}$. The efficacy of the modified electrode for electrocatalytic H_2-generation was evaluated based on 1 h CPE of the freshly prepared 1 M $KCl_{(aq)}$ at an applying potential −1.2 V (vs. SHE; Supporting Information, Figure S13 D, E). As opposed to the negligible reactivity of the electrode deposited with free amine ligands or Fe complexes with no NO ligands, electrocatalytic reactivity for H_2-generation of the modified electrode follows the order of 2-PMDTA > 1-TMEDA > 2-DTA, which is consistent with the homogenous study described above. An onset potential of −0.98 V (vs. SHE) exhibited by "direct deposit of DNIC 2-PMDTA" on the electrode, by physical adsorption presumably, demonstrates that the "electrodeposit of 2-PMDTA" together with iron metal and iron oxide results in the efficient HER reactivity of the 2-PMDTA-deposited electrode (Table 1; Supporting Information, Figure S13C).

The distinctive HER reactivity of the robust Pt electrode designates itself as a standard reference for the development of solid-state hydrogen evolution cathode in industrial applications. Table 1 summarizes the onset potential for HER, applying potential required to achieve 10 and 20 mA cm^{-2}, and Tafel slope for a 2-PMDTA-deposited electrode and Pt electrode in 1 M $KCl_{(aq)}$. The linear sweep voltammetry (LSV) curve of the 2-PMDTA-deposited electrode exhibits an onset potential of −0.717 V (vs SHE; Figure 3 A), which is comparable to the onset potential of Pt electrode of −0.673 V (vs SHE). Utilization of 1 M KCl or 1 M Na_2SO_4 as the electrolyte shows no significant difference according to the similar LSV curve of the 2-PMDTA-deposited electrode in 1 M $KCl_{(aq)}$ or 1 M $Na_2SO_{4(aq)}$ (Supporting Information, Figure S14). Importantly, the Tafel slope of 202 mV dec^{-1} for the 2-PMDTA-deposited electrode is smaller than that for Pt (242 mV dec^{-1} as determined in the range of −820 and −920 mV vs SHE; Figure 3 B). The current density of 10 and 20 mA cm^{-2} are obtained under the potentials of −0.787 and −0.845 V (vs SHE), individually, for the 2-PMDTA-deposited electrode, compared to the potentials of −0.843 and −0.921 V (vs SHE) for Pt (Table 1). Also, a current density of 215 mA cm^{-2} observed in the electrolysis of 1 M $KCl_{(aq)}$ using the 2-PMDTA-deposited electrode at an applied potential of −1.2 V (vs SHE) for 1 h is higher than that of 65 mA cm^{-2} when Pt electrode is used (Supporting Information, Figure S15). It is concluded that the electrocatalytic reactivity of 2-PMDTA-deposited electrode for HER under neutral and basic conditions is comparable to Pt (Supporting Information, Table S3).[8a,9,29]

Table 1: Comparisons of the onset potentials, required potentials to achieve current density of 10 and 20 mA/cm^2, and Tafel slope between the 2-PMDTA-deposited electrode and Pt electrode in 1 M $KCl_{(aq)}$.

Electrode	Onset Potential [V]	Potential for [×10 mA cm^{-12}] [V]	Potential for [×20 mA cm^{-2}] [V]	Tafel Slope [mV dec^{-1}]
2-PMDTA deposited	−0.717	−0.787	−0.845	202
Pt	−0.673	−0.843	−0.921	242

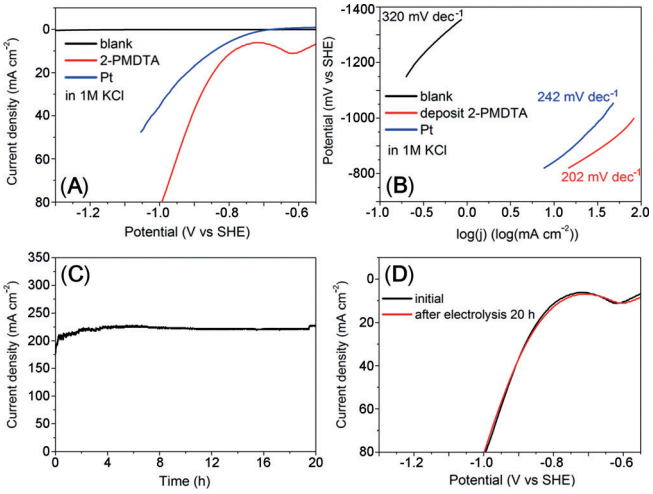

Figure 3. A) Linear sweep voltammetry (LSV) curves and B) the corresponding Tafel plots of glassy carbon (black), 2-PMDTA-deposited electrode (red) and Pt (blue) in 1.0 M $KCl_{(aq)}$, respectively. Scan rate: 50 mV s^{-1}. C) Current density for the electrolysis of 1 M $KCl_{(aq)}$ using 2-PMDTA-deposited electrode at an applied potential of −1.2 V (vs SHE) for 20 h. D) Linear sweep voltammetry (LSV) curves of the freshly prepared 2-PMDTA-deposited electrode (black) and the 2-PMDTA-deposited electrode used as HER in 1 M $KCl_{(aq)}$ at an applied potential of −1.2 V (vs SHE) for 20 h (red). Scan rate: 50 mV s^{-1}.

During the extended CPE of 1M $KCl_{(aq)}$ using the 2-PMDTA-deposited electrode at an applying potential −1.2 V (vs. SHE) for 20 h, a stable current density was observed (Figure 3C). Furthermore, the complete overlap of LSVs between the freshly prepared 2-PMDTA-deposited electrode and the 2-PMDTA-deposited electrode used for 20 h indicates that 2-PMDTA-deposited electrodes can serve as a robust electrode for HER (Figure 3D). The extended electrolysis of the 2-PMDTA-deposited electrode for 139 h shows steady charge consumption (total 8696 Coulomb) for generation of H_2 with an average current density of 246 $mA\,cm^{-2}$ (Supporting Information, Figure S16). The weight of 2-PMDTA-deposit on the surface of the glassy carbon disk is estimated as 0.3 mg. Accordingly, the turnover number (TON) and turnover frequency (TOF) are calculated as 150.2 $mol\,g^{-1}$ and 1.08 $mol\,g^{-1}\,h^{-1}$, respectively. The LSVs of the 2-PMDTA-deposited electrode and Pt electrode in 1M $KCl_{(aq)}$ and 1M $NaOH_{(aq)}$, respectively, show a cross point at a potential of −0.975 V and −0.895 V (vs SHE; Supporting Information, Figure S17). That is, 2-PMDTA-deposited electrode features a better HER reactivity under basic condition at higher applying potential and rationalizes the increase of current density with time in the extended electrolysis of 1M $KCl_{(aq)}$ for 139 h using 2-PMDTA-deposited electrode (Supporting Information, Figures S16, S18).

In summary, the accessibility of multiple redox states modulated by the non-innocent NO-coordinate ligands and the pendant amine as a proton relay for 2-PMDTA work in concert to achieve efficient catalytic water reduction. 2-PMDTA has shown promise as a low-cost precursor to assemble $[Fe(NO)_2]$ motif onto electrodes through a facile electrodeposition process. Herein, we demonstrate the modification of a molecular catalyst to a solid-state hydrogen evolution cathode. Compared to Pt electrode, the 2-PMDTA-deposited electrode enjoins the higher onset potential, but features the smaller Tafel slope in 1M KCl. Systematic optimization of molecular catalysts with parallel efforts made on deposit of it on electrode open an avenue for design of catalytic materials. This discovery raises a broad interest in the utilization of the $[Fe(NO)_2]$ motif as a translational molecular platform for practical H_2-generation, while the study of conjugation with solar energy and retrieving electrons from water is underway.

Acknowledgements

We gratefully acknowledge financial support from the Ministry of Science and Technology (Taiwan). We thank Ms. Yun-Ming Li (NCTU) and Ms. Swee Lan Cheah (NTHU) for the help on elemental analysis and XPS experiments, also, Mr. Ting-Shen Kuo (NTNU) and Ms. Pei-Lin Chen (NTHU) for the single-crystal X-ray structural determinations.

Keywords: electrocatalysis · hydrogen · iron · nitric oxide · water reduction

How to cite: *Angew. Chem. Int. Ed.* **2015**, *54*, 14824–14829
Angew. Chem. **2015**, *127*, 15037–15042

[1] J. A. Turner, *Science* **1999**, *285*, 687–689.
[2] J. C. Fontecilla-Camps, A. Volbeda, C. Cavazza, Y. Nicolet, *Chem. Rev.* **2007**, *107*, 4273–4303.
[3] L. Chen, M. Wang, K. Han, P. Zhang, F. Gloaguen, L. Sun, *Energy Environ. Sci.* **2014**, *7*, 329–334.
[4] J. N. Butt, M. Filipiak, W. R. Hagen, *Eur. J. Biochem.* **1997**, *245*, 116–122.
[5] a) D.-Y. Wang, M. Gong, H.-L. Chou, C.-J. Pan, H.-A. Chen, Y. Wu, M.-C. Lin, M. Guan, J. Yang, C.-W. Chen, Y.-L. Wang, B.-J. Hwang, C.-C. Chen, H. Dai, *J. Am. Chem. Soc.* **2015**, *137*, 1587–1592; b) P. Jiang, Q. Liu, Y. Liang, J. Tian, A. M. Asiri, X. Sun, *Angew. Chem. Int. Ed.* **2014**, *53*, 12855–12859; *Angew. Chem.* **2014**, *126*, 13069–13073; c) M. Tavakkoli, T. Kallio, O. Reynaud, A. G. Nasibulin, C. Johans, J. Sainio, H. Jiang, E. I. Kauppinen, K. Laasonen, *Angew. Chem. Int. Ed.* **2015**, *54*, 4535–4538; *Angew. Chem.* **2015**, *127*, 4618–4621.
[6] a) Y. Sun, C. Liu, D. C. Grauer, J. Yano, J. R. Long, P. Yang, C. J. Chang, *J. Am. Chem. Soc.* **2013**, *135*, 17699–17702; b) S. Du, Z. Ren, J. Zhang, J. Wu, W. Xi, J. Zhu, H. Fu, *Chem. Commun.* **2015**, *51*, 8066–8069; c) N. Jiang, B. You, M. Sheng, Y. Sun, *Angew. Chem. Int. Ed.* **2015**, *54*, 6251–6254; *Angew. Chem.* **2015**, *127*, 6349–6352; d) J. Wang, D. Gao, G. Wang, S. Miao, H. Wu, J. Li, X. Bao, *J. Mater. Chem. A* **2014**, *2*, 20067–20074; e) H. Yan, C. Tian, L. Wang, A. Wu, M. Meng, L. Zhao, H. Fu, *Angew. Chem. Int. Ed.* **2015**, *54*, 6325–6329; *Angew. Chem.* **2015**, *127*, 6423–6427.
[7] a) M. Gong, W. Zhou, M.-C. Tsai, J. Zhou, M. Guan, M.-C. Lin, B. Zhang, Y. Hu, D.-Y. Wang, J. Yang, S. J. Pennycook, B.-J. Hwang, H. Dai, *Nat. Commun.* **2014**, *5*, 4695; b) X. Wang, Y. V. Kolen'ko, X. Q. Bao, K. Kovnir, L. Liu, *Angew. Chem. Int. Ed.* **2015**, *54*, 8188–8192; *Angew. Chem.* **2015**, *127*, 8306–8310.
[8] a) Q. Lu, G. S. Hutchings, W. Yu, Y. Zhou, R. V. Forest, R. Tao, J. Rosen, B. T. Yonemoto, Z. Cao, H. Zheng, J. Q. Xiao, F. Jiao, J. G. Chen, *Nat. Commun.* **2015**, *6*, 6567; b) J. Q. Tian, Q. Liu, N. Y. Cheng, A. M. Asiri, X. P. Sun, *Angew. Chem. Int. Ed.* **2014**, *53*, 9577–9581; *Angew. Chem.* **2014**, *126*, 9731–9735.
[9] a) T. F. Jaramillo, K. P. Jørgensen, J. Bonde, J. H. Nielsen, S. Horch, I. Chorkendorff, *Science* **2007**, *317*, 100–102; b) M.-R. Gao, J.-X. Liang, Y.-R. Zheng, Y.-F. Xu, J. Jiang, Q. Gao, J. Li, S.-H. Yu, *Nat. Commun.* **2015**, *6*, 5982; c) H. B. Wu, B. Y. Xia, L. Yu, X. Y. Yu, X. W. Lou, *Nat. Commun.* **2015**, *6*, 6515.
[10] F. Gloaguen, J. D. Lawrence, T. B. Rauchfuss, *J. Am. Chem. Soc.* **2001**, *123*, 9476–9477.
[11] C. Tard, C. J. Pickett, *Chem. Rev.* **2009**, *109*, 2245–2274.
[12] a) R. Mejia-Rodriguez, D. Chong, J. H. Reibenspies, M. P. Soriaga, M. Y. Darensbourg, *J. Am. Chem. Soc.* **2004**, *126*, 12004–12014; b) C.-H. Hsieh, S. Ding, O. F. Erdem, D. J. Crouthers, T. Liu, C. C. L. McCrory, W. Lubitz, C. V. Popescu, J. H. Reibenspies, M. B. Hall, M. Y. Darensbourg, *Nat. Commun.* **2014**, *5*, 3684.
[13] M. L. Helm, M. P. Stewart, R. M. Bullock, M. R. DuBois, D. L. DuBois, *Science* **2011**, *333*, 863–866.
[14] V. S. Thoi, Y. J. Sun, J. R. Long, C. J. Chang, *Chem. Soc. Rev.* **2013**, *42*, 2388–2400.
[15] P. W. Du, R. Eisenberg, *Energy Environ. Sci.* **2012**, *5*, 6012–6021.
[16] a) W. M. Singh, T. Baine, S. Kudo, S. Tian, X. A. N. Ma, H. Zhou, N. J. DeYonker, T. C. Pham, J. C. Bollinger, D. L. Baker, B. Yan, C. E. Webster, X. Zhao, *Angew. Chem. Int. Ed.* **2012**, *51*, 5941–5944; *Angew. Chem.* **2012**, *124*, 6043–6046; b) Y. Sun, J. P. Bigi, N. A. Piro, M. L. Tang, J. R. Long, C. J. Chang, *J. Am. Chem. Soc.* **2011**, *133*, 9212–9215; c) B. D. Stubbert, J. C. Peters, H. B. Gray, *J. Am. Chem. Soc.* **2011**, *133*, 18070–18073.
[17] a) H. I. Karunadasa, E. Montalvo, Y. Sun, M. Majda, J. R. Long, C. J. Chang, *Science* **2012**, *335*, 698–702; b) H. I. Karunadasa, C. J. Chang, J. R. Long, *Nature* **2010**, *464*, 1329–1333.

[18] a) A. D. Das, Z. Han, W. W. Brennessel, P. L. Holland, R. Eisenberg, *ACS Catal.* **2015**, *5*, 1397 – 1406; b) O. R. Luca, S. J. Konezny, J. D. Blakemore, D. M. Colosi, S. Saha, G. W. Brudvig, V. S. Batista, R. H. Crabtree, *New J. Chem.* **2012**, *36*, 1149 – 1152; c) P. Zhang, M. Wang, Y. Yang, T. Yao, L. Sun, *Angew. Chem. Int. Ed.* **2014**, *53*, 13803 – 13807; *Angew. Chem.* **2014**, *126*, 14023 – 14027.

[19] a) J. Kibsgaard, T. F. Jaramillo, F. Besenbacher, *Nat. Chem.* **2014**, *6*, 248 – 253; b) E. S. Andreiadis, *Nat. Chem.* **2013**, *5*, 48 – 53.

[20] F.-T. Tsai, S.-J. Chiou, M.-C. Tsai, M.-L. Tsai, H.-W. Huang, M.-H. Chiang, W.-F. Liaw, *Inorg. Chem.* **2005**, *44*, 5872 – 5881.

[21] M.-C. Hung, M.-C. Tsai, G.-H. Lee, W.-F. Liaw, *Inorg. Chem.* **2006**, *45*, 6041 – 6047.

[22] J. H. Enemark, R. D. Feltham, *Coord. Chem. Rev.* **1974**, *13*, 339 – 406.

[23] T.-T. Lu, S.-H. Lai, Y.-W. Li, I.-J. Hsu, L.-Y. Jang, J.-F. Lee, I.-C. Chen, W.-F. Liaw, *Inorg. Chem.* **2011**, *50*, 5396 – 5406.

[24] M.-C. Tsai, F.-T. Tsai, T.-T. Lu, M.-L. Tsai, Y.-C. Wei, I.-J. Hsu, J.-F. Lee, W.-F. Liaw, *Inorg. Chem.* **2009**, *48*, 9579 – 9591.

[25] T.-T. Lu, T.-C. Weng, W.-F. Liaw, *Angew. Chem. Int. Ed.* **2014**, *53*, 11562 – 11566; *Angew. Chem.* **2014**, *126*, 11746 – 11750.

[26] M.-L. Tsai, C.-C. Tsou, W.-F. Liaw, *Acc. Chem. Res.* **2015**, *48*, 1184 – 1193.

[27] a) A. Le Goff, V. Artero, B. Jousselme, P. D. Tran, N. Guillet, R. Métayé, A. Fihri, S. Palacin, M. Fontecave, *Science* **2009**, *326*, 1384 – 1387; b) D. Merki, X. Hu, *Energy Environ. Sci.* **2011**, *4*, 3878 – 3888; c) S. Cobo, J. Heidkamp, P.-A. Jacques, J. Fize, V. Fourmond, L. Guetaz, B. Jousselme, V. Ivanova, H. Dau, S. Palacin, M. Fontecave, V. Artero, *Nat. Mater.* **2012**, *11*, 802 – 807; d) M. W. Kanan, D. G. Nocera, *Science* **2008**, *321*, 1072 – 1075; e) J. D. Blakemore, M. W. Mara, M. N. Kushner-Lenhoff, N. D. Schley, S. J. Konezny, I. Rivalta, C. F. A. Negre, R. C. Snoeberger, O. Kokhan, J. Huang, A. Stickrath, L. A. Tran, M. L. Parr, L. X. Chen, D. M. Tiede, V. S. Batista, R. H. Crabtree, G. W. Brudvig, *Inorg. Chem.* **2013**, *52*, 1860 – 1871; f) J. M. Thomsen, S. W. Sheehan, S. M. Hashmi, J. Campos, U. Hintermair, R. H. Crabtree, G. W. Brudvig, *J. Am. Chem. Soc.* **2014**, *136*, 13826 – 13834.

[28] S. W. Sheehan, J. M. Thomsen, U. Hintermair, R. H. Crabtree, G. W. Brudvig, C. A. Schmuttenmaer, *Nat. Commun.* **2015**, *6*, 6469.

[29] X. Zou, X. Huang, A. Goswami, R. Silva, B. R. Sathe, E. Mikmeková, T. Asefa, *Angew. Chem. Int. Ed.* **2014**, *53*, 4372 – 4376; *Angew. Chem.* **2014**, *126*, 4461 – 4465.

Received: September 7, 2015
Published online: October 6, 2015

